Amorphous magnetism in Fe-B alloys: First-principles spin-polarized electronic-structure calculations

J. Hafner
Institut für Theoretische Physik, Technische Universität Wien, Wiedner Hauptstrasse 8-10, A-1040 Wien, Austria

M. Tegze
Institut für Theoretische Physik, Technische Universität Wien, Wiedner Hauptstrasse 8-10, A-1040 Wien, Austria and Central Research Institute for Physics, Hungarian Academy of Sciences, H 1525 Budapest, Hungary

Ch. Becker
Institut für Theoretische Physik, Technische Universität Wien, Wiedner Hauptstrasse 8-10, A-1040 Wien, Austria
(Received 26 August 1993)

We present self-consistent spin-polarized electronic-structure calculations for amorphous Fe_xB_{100-x} ($50 \leq x \leq 95$) alloys, based on a supercell linear-muffin-tin-orbital technique and realistic structure models produced by molecular-dynamics simulations. We show that the electronic densities of states of the amorphous alloys are very similar to that of the crystalline Fe borides. This confirms the conclusions as to the similarity of the local order in the crystalline and amorphous phases drawn on the basis of the structural studies. The calculated composition dependence of the magnetic moments is in good agreement with experimental data on amorphous films, with a maximum of the magnetic moment close to 15 at. % B. The decrease of the moment for lower B content is shown to arise from the competition between ferro- and antiferromagnetic exchange interactions, the decrease with higher B content is due to a dilution effect: polarizable *d-d* bonds are replaced by magnetically inert *p-d* bonds. We also present detailed calculations of the photoemission intensities.

I. INTRODUCTION

During the last decades, a vast literature has been devoted to the magnetic properties of amorphous transition-metal–metalloid alloys.[1] The two competing theoretical concepts for the magnetism of alloys (the band theory based on a picture of nearly free itinerant electrons[2,3] and the Heisenberg model of localized spins[4,5]) have also been applied to amorphous magnets. On the basis of the concept of localized electrons Corb *et al.*[6] have developed the "coordination-bond model" which attributes the reduction of the magnetic moments with an increasing content of metalloid atoms to the chemical bonding, i.e., to the formation of nonpolarizable *p-d* hybrid bonds from polarizable 3*d* transition-metal states. On the other hand, Malozemoff *et al.*[7,8] developed the "band-gap theory" of strong ferromagnetism in amorphous alloys based on the existence of a hybridization gap in the electronic density of states in the majority-spin band. Whereas the coordination-bond model focuses on the local atomic environment, and especially on the metal neighbors of the metalloid atoms, the band-gap theory asserts that the reduction of the magnetic moment is determined only by the valence of the metalloid and is independent of the local environment. However, a critical analysis[9] of the magnetization data of amorphous (Fe,Co,Ni)-(B,P) alloys shows that neither the band-gap model nor the coordination-bond model offer a consistent explanation of the composition dependence of ferromagnetism. The striking contrast between Co- and Fe-based alloys is very instructive: In amorphous Co-B and Co-P alloys (as well as in Co-based amorphous transition-metal alloys), the average magnetic moment per Co atom varies almost linearly with composition.[10] The magnetic moment in the amorphous alloys is almost the same as in the crystalline compounds and, for low metalloid content, extrapolates to the magnetic moment of pure Co. The alloys show strong magnetism and only weak magnetovolume effects. On the other hand, amorphous Fe-B, Fe-P, Fe-Zr, Fe-Y,... alloys show a maximum of the magnetic moment at approximately 85 at. % Fe.[10–15] The strong magnetovolume effect observed in the Fe-based alloys and the Invar effect are strongest at the composition with the largest magnetic moment. In the Fe-rich regime, the data show rather strong scatter, depending on the preparation conditions and on the thermal history of the samples. As a rule, the magnetic moments are lower in vapor-quenched amorphous ribbons[11,14] and decrease faster with decreasing B concentration. Only for microcrystalline alloys does the magnetic moment of the Fe-rich alloys extrapolate to the magnetic moment of α-Fe ($\mu \simeq 2.2\mu_B$). For the amorphous alloys, the moment extrapolates to the much lower value ascribed to hypothetical amorphous Fe ($\mu \simeq 1.3\mu_B - 1.5\mu_B$).[16] For higher B content, the magnetic moment in the amorphous alloys is only slightly lower than that of the crystalline Fe borides.[14]

There have been several electronic-structure calculations for the amorphous Fe borides.[17–21] The calculations of Fujiwara[17] and of Nowak *et al.*[18] are based on the tight-binding linear-muffin-tin-orbital (TB-LMTO) method[22] and simple structural models based on relaxed dense-random-packing structures. The calculations are for the paramagnetic phase and achieve self-consistency

only in an average sense (one-electron potential and charge density are consistent for average Fe and B sites). The tight-binding calculations of Krompiewski *et al.*[19] and Ching and Xu[20] and the TB-LMTO calculations of Turek[21] have been performed for the ferromagnetic phase, but they are either non-self-consistent[20,21] or achieve self-consistency only between spin density and magnetic moments, at fixed interatomic transfer integrals.[19] Krompiewski *et al.*[19] and Turek[21] made an attempt to study the variation of the magnetic moment with composition and achieved reasonable agreement with the rather scattered experimental data for B contents larger than 15 at. %. The Fe-rich region has been explored only by Krompiewski *et al.*; the magnetic moments extrapolate to a very low value ($\mu \simeq 1.1\mu_B$) in hypothetical amorphous iron. No serious attempt has been made to correlate the predictions for the electronic structure with existing data: The paramagnetic results[17,18] for the electronic specific heat disagree with experiment[23] by up to a factor of 3; the comparison with photoemission[24–27] and soft x-ray spectra[28,29] is hampered by the scatter between the various sets of experimental data and the evident importance of matrix-element and resolution effects.

Thus, in spite of the evident technological importance of the materials, our understanding of their electronic and magnetic behavior is still at a surprisingly low level. The key to progress seems to be in the resolution of two problems: (a) improved structural modeling. A good structural model should predict not only the average structure factor, but, much more importantly, the partial structure factors at a level of detail sufficient to characterize the chemical and topological short- and medium-range order. Furthermore, the modeling should be based on interatomic forces based on a quantum-mechanical description of the chemical bond to allow one to check the consistency of the atomic and electronic structures. (b) The other problem is electronic structure calculations that are self-consistent not only on average, but achieve consistency between the *local* potential and the local charge and spin density on the individual atomic sites.

Recently, it has been shown that the key to a calculation of interatomic forces in materials with an appreciable covalent character of the chemical bond is in the revival of an old concept: the bond order.[30,31] Within tight-binding theory, the total energy may be decomposed in a repulsive pairwise term (describing the electrostatic and exchange-correlation contributions) and a covalent bond energy with the strength of each bond given by the product of the transfer integral and the bond order counting the difference in the number of electrons in bonding and antibonding states. Different methods for the calculation of the bond order have been proposed.[32–34] For disordered materials, the analytical calculation of the bond order on a Bethe lattice used as a reference system has proven to be particularly fruitful.[33,34] A Bethe lattice is characterized only by the mean bond length and coordination number, but this turns out to be sufficient to grasp the essential aspects of the electronic structure. For example, for transition-metal glasses this simplified approach reflects the change from weak, additive interatomic forces in the common-band alloys (e.g., in Ni-Pd) to strong, nonadditive forces in split-band alloys (e.g., Ni-Zr, Ni-Y). The tight-binding-bond approach has very recently been generalized to transition-metal–metalloid alloys[35] and it has been shown that the resulting nonadditive potentials lead to a very accurate description of the chemical and topological short- and medium-range order.[35,36]

For the calculation of the electronic properties of liquid and amorphous metals, the supercell method[37,38] is the only one to achieve local self-consistency. In the supercell method, the glass is modeled by a small, periodically repeated supercell. It has been shown[39] that supercells containing 60–70 inequivalent atomic sites yield a reliable description of the electronic density of states of the amorphous alloy, which is not seriously affected by the periodic boundary conditions. Larger supercells containing ~ 150 atoms are sufficient for the calculation of transport properties.[40] The supercell method has also been extended to spin-polarized electronic-structure calculations.[41,42]

In this paper we present spin-polarized electronic-structure calculations for amorphous Fe_xB_{100-x} alloys, for compositions ranging from pure Fe to the monoboride FeB. Our calculations are based on accurate structural models generated using a simulated molecular-dynamics quench and tight-binding-bond potentials. We use a linear-muffin-tin-orbital (LMTO) supercell technique which permits for locally self-consistent calculations and present a detailed analysis of spin-polarized photoemission intensities. We find that in the Fe-rich limit, the magnetic properties are dominated by competing ferro- and antiferromagnetic exchange interactions arising from local fluctuations in the potentials and charge densities. The presence of antiferromagnetic exchange interactions leads to the appearance of negative Fe moments for isolated sites, causing the decrease of the average moment at B contents lower than 15 at. %. These effects are strongly volume dependent. At larger B contents the saturation moment decreases again; in an amorphous $Fe_{50}B_{50}$ alloy most iron atoms are nonmagnetic ($\sim 2/3$), and the others show moments fluctuating between $0.2\mu_B$ and $1.2\mu_B$. This is in contrast to the crystalline monoboride with a magnetic moment of about $1.2\mu_B$ per Fe atom. We show that the faster decrease of the magnetic moment with increasing B content is largely disorder induced. We also present detailed calculations of the x-ray and ultraviolet photoemission spectra and a detailed comparison with experimental data.

The paper is organized as follows: In Sec. II we recapitulate very briefly the construction of the structural models; Sec. III describes the technical details of the self-consistent local spin-density calculations using the LMTO method. Section IV presents the results and contains a detailed discussion of the structure-property relationship. Our conclusions are presented in Sec. V.

II. STRUCTURAL MODELING

Our calculations are based in the structural models of Ref. 35, extended to a wide range of compositions. The

models are generated by a simulated molecular-dynamics quench based on interatomic forces derived using a tight-binding-bond approach from a simplified model of the electronic structure. The basic assumption of a narrow Fe-*d* band interacting with a broad B-*p* band is motivated by our knowledge of the electronic structure of the crystalline Fe-B phases.[43–45] The forces mediated by the covalent bond in the *p-d* band complex are expressed in terms of the tight-binding transfer integral $t_{ij}(R)$ and the bond order Θ_{ij} counting the difference in the number of electrons occupying bonding and antibonding states. The bond order may be expressed in terms of the off-diagonal Green's function and calculated analytically using renormalized perturbation theory on a Bethe-lattice-reference system. The contribution of the Fe-*s* electrons to the interatomic forces is treated via pseudopotential perturbation theory; the B-*s* electrons are assumed to form a completely filled nonbonding band interacting only weakly with the *p-d* bands. The results of the present paper largely confirm these assumptions. The tight-binding-bond method leads to strongly nonadditive pair forces with a preference for strong, short Fe-B bonds. This nonadditivity reflects the strong covalent character of the bond and is the main cause for the observed chemical and topological short- and medium-range order effects. The simulations used for the analysis of the diffraction data are based on ensembles with $N=10^3$ to 2×10^4 atoms.[35,36] To generate the coordinates for the electronic-structure calculations, the molecular-dynamics simulations are repeated for $N=64$ atom ensembles. Configurations for the electronic-structure calculations were chosen such that the partial correlation functions calculated for a single 64-atom configuration are as close as possible to those derived from an ensemble average of over the larger models. For any further details and for a detailed comparison of the calculated structure with experiment we refer the reader to Refs. 35 and 36. Here we only emphasize the close similarity of the short-range chemical and topological order of the amorphous alloys with the trigonal-prismatic atomic arrangements in crystalline Fe_xB, $x=1,2,3$, demonstrated in these simulations.

III. ELECTRONIC STRUCTURE: COMPUTATIONAL DETAILS

The techniques for calculating the electronic structure of amorphous solids fall essentially into three classes: (i) effective medium approaches, (ii) supercell techniques, and (iii) real-space recursion calculations. Effective medium approaches[46] attempt to extend the coherent-potential theory (which has been very successful for substitutionally disordered alloys) to the case of topologically disordered materials. They involve very complex averages over complex many-body correlation functions and have never been shown to work beyond the most simple monatomic cases. Supercell techniques apply conventional band-structure methods developed for crystalline solids to periodically repeated supercells representing the amorphous material.[37–39] The advantage of the supercell techniques is that they allow to achieve charge self-consistency on every local site; the disadvantage is that the application of the technique is in practice limited to systems with a maximum of 100 inequivalent sites in the periodically repeated cell. The real-space recursion method is based on a tight-binding representation of the Hamiltonian. In non-self-consistent calculations, very large systems (up to 10^4 atoms) may be treated. However, to achieve charge self-consistency, the local density of states (DOS) on every site is required. In practice, self-consistency is achieved only for an average atom represented by the local DOS and charge density averaged over a small number of atoms (typically 10–20) selected from the central region of a larger cluster (typically 500–1000 atoms).[17,18] Comparing the recursion and supercell methods, the advantage of the former is that it is less affected by the periodic boundary conditions and that of the latter is the possibility to achieve local self-consistency. Comparisons of supercell calculations with $\sim$60 atoms per cell with recursion calculations based on 800-atom clusters representing amorphous $Ca_{70}Al_{30}$ have demonstrated that the effect of the periodic boundary is small.[39] On the other hand it can be shown that the neglect of self-consistency effects on the local fluctuations in the charge density and in the potential can lead to substantial differences in the local DOS and in the local magnetic moments.[47] So in applications whose aim it is to explore the relation between the local atomic and the local magnetic structure, there is no alternative to the use of the supercell method.

In principle, any band-structure code could be used for supercell calculations—the choice is merely a matter of computational efficiency. In our calculations we used the scalar relativistic variant of the linear-muffin-tin-orbital (LMTO) method[48] in the atomic-sphere approximation (ASA). Exchange and correlations are treated in the local-spin-density approximation (LSDA).[49] The ratio of the radii of the atomic spheres is taken as $r_B/r_{Fe}=0.82$, corresponding to the positions of the nearest-neighbor peaks in the Fe-B and Fe-Fe correlation functions. A supercell represents only one possible atomic configuration—in principle a configuration average must be performed. This is a very expensive procedure. We have taken an average over a small number of configurations for the example of $Fe_{80}B_{20}$ and found that the configuration-induced changes in the total DOS are very small. In the average magnetic moment we found changes of $\pm3\%$, depending on configuration. For most other compositions, only a single reference configuration has been considered.

Photoemission intensities are calculated in terms of the partial photoionization cross sections $\sigma_{\alpha\sigma l}(\hbar\omega,E)$ and the partial densities of states $n_{\alpha\sigma l}(E)$ (α=Fe,B). The partial photoionization cross sections are calculated under the following approximations: (a) neglect of wave-vector conservation (as is legitimate for amorphous materials), (b) dipole approximation to the electromagnetic field, and (c) single-scatterer final-state approximation.[50,51]

IV. ELECTRONIC AND MAGNETIC STRUCTURE

The calculations have been performed at the atomic densities of the amorphous alloys given by Hasegawa and

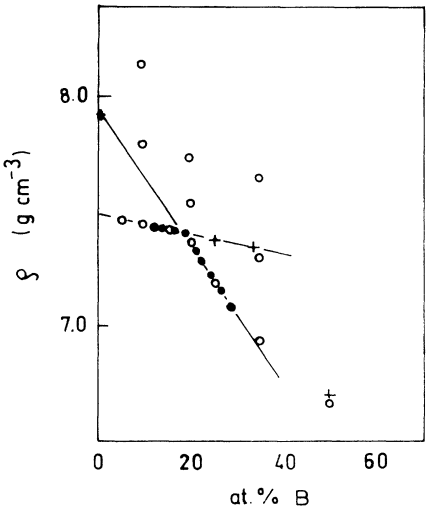

FIG. 1. Composition dependence of the density of amorphous Fe_xB_{100-x} alloys and of crystalline Fe-B compounds. (●) experimental data of Hasegawa and Ray (Ref. 52) for glassy alloys, (+) experimental densities for pure Fe and crystalline Fe_3B, Fe_2B, and Fe-B (Ref. 55), and (○) densities used in the present calculations.

Ray.[52] The determination of the density of amorphous alloys is always subject to some uncertainty, experimentally as well as in computer simulations. The data of Hasegawa and Ray show a marked change in slope at about 21 at.% B (see Fig. 1): The approximately linear concentration dependence in the Fe-rich regime extrapolates to a density of $\rho \sim 7.47$ g cm^3, about 6% lower than the density of bcc Fe ($\rho = 7.92$ g cm^{-3}). At higher B content the density varies again approximately linearly with composition—this time the linear trend extrapolates to the density of crystalline iron. This change in the concentration dependence of the density has been taken to indicate a change in the atomic structure.[53] Recent computer simulations[36] have confirmed that the medium-range order in the glassy phase changes profoundly as the composition approaches that of the crystalline Fe_3B phase. The density of the crystalline compounds[54] is always substantially larger than that of the amorphous alloys (the difference is up to 5.5% in the case of Fe_2B). In our calculations, we have used densities that interpolate (respectively slightly extrapolate) the data of Hasegawa and Ray. In addition we have investigated the density dependence of the electronic and magnetic properties for a few selected compositions.

A. Electronic density of states and distribution of magnetic moments

Figure 2 shows the spin-polarized electronic densities of states for amorphous Fe_xB_{100-x} alloys with $50 \leq x \leq 95$; Fig. 3 shows the distributions of the local magnetic moments for these alloys. These are the main results of this paper. The electronic DOS of the glassy alloys is surprisingly close to that of the corresponding crystalline phases:[43–45] The electronic states close to the Fermi level are dominated by the Fe-*d* states forming a spin-split two-peaked band with the Fermi level just above the main peak of the majority band and close to the minimum of the DOS in the minority band. A remarkable difference in the DOS's of the crystalline and amorphous alloys is the absence of the hybridization gap at the upper edge of the *d* band in the amorphous phases. For all amorphous alloys, the Fermi level falls in a region of rapidly decreasing DOS, in contrast to the crystalline compounds where E_F is pinned in the hybridization gap.[8,43–45] The similarity in the two-peak structure of the DOS of the crystalline and amorphous alloys is important, because it demonstrates that the structure of the DOS of the amorphous alloy is not related to the two-peak structure of the DOS of elemental bcc Fe (fcc or hcp Fe have a totally different DOS structure). The latter originates from the atomic arrangement in the bcc lattice with eight nearest neighbors arranged on a cube and six next-nearest neighbors arranged on an octahedron. The crystalline Fe-B compounds are characterized by local units in the form of a B-centered trigonal prism of Fe atoms, eventually with additional Fe atoms capping the square faces of the prism. Our simulations have shown[35,36] that this is also the preferred local order in the amorphous alloys. Therefore the double-peaked DOS of the amorphous Fe-B alloys does not indicate a local bcc-like coordination, but the similarity of the local order in the crystalline and amorphous phases.

Of the previous electronic-structure calculations for *a*-Fe_xB_{100-x} alloys, the real-space recursion calculations using the TB-LMTO calculations of Nowak *et al.*[18] (paramagnetic) and Bratkovsky and Smirnov[60] (spin polarized) for $Fe_{80}B_{20}$ show the double-peaked structure of the DOS, but not the spin-polarized empirical TB calculation of Krompiewski *et al.*[19] This could indicate the importance of charge self-consistency (although this is achieved only in an average way in the recursion calculations).

The analysis of the partial local DOS's (Fig. 4) shows several remarkable features: (i) The B-*s* states interact only weakly with the Fe-*d*–B-*p* band complex. B-*s* and B-*p* states are separated by a remarkably distinct pseudogap at a binding energy of 7–8 eV (depending slightly on composition). The *s* states form a fully occupied, nonbonding band. This confirms the assumptions made in the construction of the tight-binding-bond potentials. Even at a composition of $Fe_{50}B_{50}$, the hybridization of B-*s* and B-*p* states is still rather weak. (ii) The covalent coupling between B-*p* and Fe-*d* states is stronger in the spin-down (minority) band, leading to a slightly increased occupation of the B spin-down states and small negative moments in the B sites. This ferrimagnetism induced by a strong covalent coupling in the spin-down band is a rather general phenomenon in many glassy and crystalline transition-metal and transition-metal–metalloid alloys.[41,42,55]

The distribution of the local magnetic moments as a function of composition is shown in Fig. 3. The Fe moments show a broad distribution of positive moments (ranging between $1\mu_B$ and $3\mu_B$ in the Fe-rich limit), with a mean value that decreases monotonically with increasing B content and with a small number of negative Fe

moments for $x \geq 85$. All B atoms carry a small negative moment (see also Table I). The most striking result is certainly the appearance of negative (antiferromagnetic) Fe moments. This correlates with the results obtained for pure amorphous Fe.[16] As for the hypothetical amorphous element this effect depends strongly on the density.

B. Magnetovolume effects: Competing ferro- and antiferromagnetic exchange interactions

For $x=90$, $x=80$, and $x=65$ we have investigated the influence of the volume on the magnetic properties. The distributions of the magnetic moments are shown in Fig. 5. In the Fe-rich alloy $Fe_{90}B_{10}$, a reduction of the atomic volume leads to a multiplication of sites with negative moments; i.e., the exchange coupling becomes more antiferromagnetic with decreasing interatomic distance. At the density of $\rho=8.15$ g cm^{-3} the distribution of the magnetic moments is bimodal; 25% of the sites carry negative moments. Even at higher B contents ($x \simeq 80$), where all Fe moments are positive at normal density, negative moments appear under compression [see Fig. 5(b)]. Only for $x=65$ does the system remain purely ferrimagnetic; compression leads only to a reduction of the overall magnetic moment. The increase of the magnetic moment with decreasing density explains the Invar effect of the

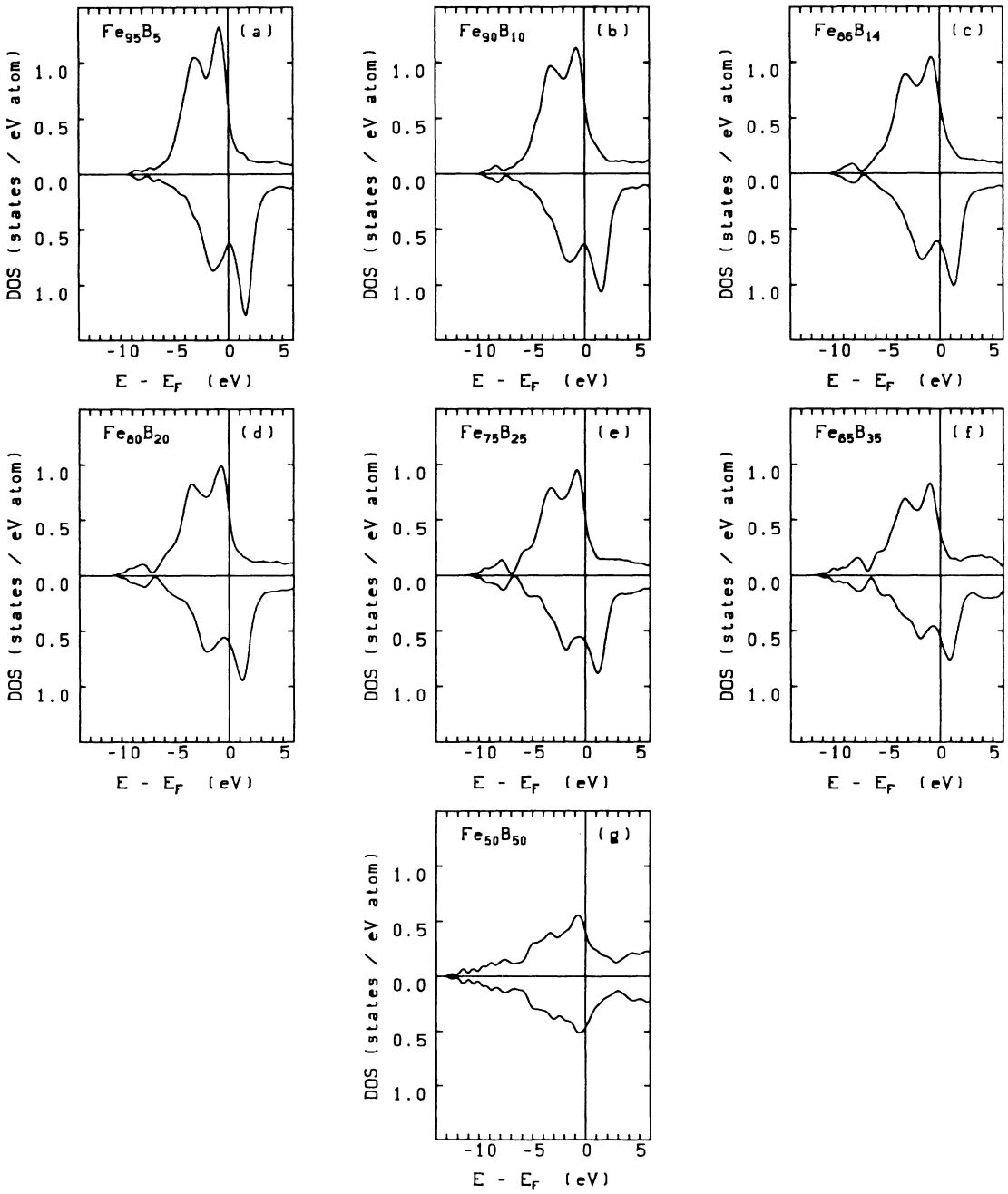

FIG. 2. Spin-polarized electronic density of states of amorphous Fe_xB_{100-x} alloys.

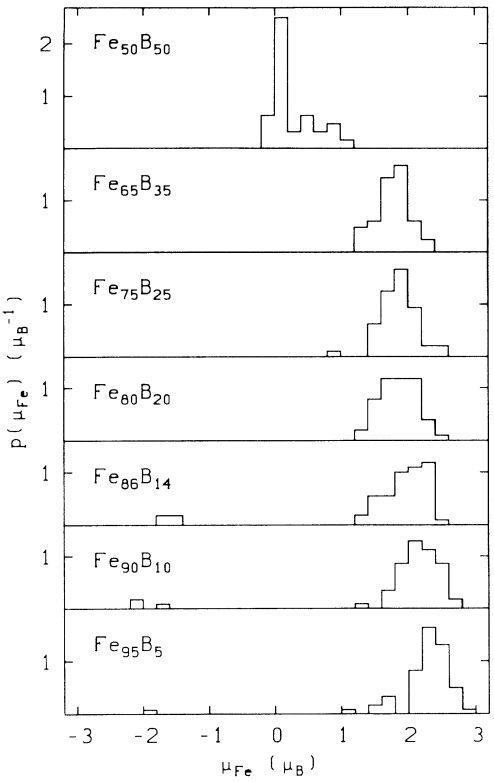

FIG. 3. Distribution of the local magnetic moments μ_{Fe} on the Fe sites in amorphous Fe_xB_{100-x} alloys.

amorphous Fe-B alloys. In agreement with experimental observation,[12] the Invar effect is the largest at the composition where the magnetic moment per Fe atom reaches a maximum, i.e., at a B content of about 20 at. %.

The same tendency towards an increasing antiferromagnetic component in the exchange interaction has been found in pure amorphous iron[16,41] and has been discussed in terms of local environment effects by Kakehashi.[56] The effect is correlated to the transition from ferromagnetism at low density to antiferromagnetism at high density in close-packed crystalline Fe. According to recent LSD calculations, this transition occurs at a nearest-neighbor distance of $d=2.575$ Å (Ref. 57), $d=2.594$ Å (Ref. 58) in fcc Fe, and $d=2.633$ Å in hcp Fe (Ref. 59). In an amorphous material, the transition from ferro- to antiferromagnetism occurs at a local level. Our detailed analysis for *a*-Fe (Ref. 16) and *a*-Fe-Zr (Ref. 41) had shown that a negative moment on a central Fe atom is stabilized, if the nearest-neighbor shell contains a high number of "contracted" neighbors (i.e., with distances ≤ 2.6 Å), in full agreement with Kakehashi's local-environment theory. This result is confirmed here for *a*-Fe-B.

It is remarkable, however, that the tight-binding calculations of Krompiewski *et al.*[19] as well as the tight-binding recursion calculations of Bratkovsky and Smirnov[60] fail to predict negative Fe moments although the average moments are in good agreement with our results. The difference is in the degree of self-consistency that has been achieved. The calculation of Krompiewski *et al.*[19] is based on an empirical tight-binding Hubbard Hamiltonian and achieves self-consistency only between exchange splitting and magnetic moment. The real-space recursion calculation of Bratkovsky and Smirnov[60] is based on a TB-LMTO Hamiltonian. Self-consistency is achieved only for an average atom: The local DOS averaged over sites taken from the central region of a cluster is used to calculate the charge density and the potential. Hence local fluctuations in the self-consistent potential are neglected. We have checked the influence of these local fluctuations by comparing TB-LMTO calculations with the locally self-consistent potentials and with the potential parameters averaged over all sites occupied with the same species. No negative moments have been found in the calculations with the averaged potential parameters. This shows that the fluctuations in the atomic environment are fully effective only if their influence on the local one-electron potential is considered. Thus local self-consistency is of prime importance for the calculation of the magnetic structure. Again these results have been confirmed for other amorphous alloys.[61]

TABLE I. Composition x, density ρ, and average magnetic moments $\bar{\mu}$ for amorphous Fe-B alloys [$\bar{\mu}=x\bar{\mu}_{Fe}+(1-x)\bar{\mu}_B$, $\bar{\mu}(Fe)=\bar{\mu}/x$, average magnetic moment per Fe atom].

	x (at. % Fe)	ρ (g cm^{-3})	$\bar{\mu}_{Fe}$ (μ_B)	$\bar{\mu}_B$ (μ_B)	$\bar{\mu}$ (μ_B)	$\bar{\mu}$(Fe) (μ_B)
$Fe_{61}B_3$	95.3	7.46	2.21	−0.15	2.10	2.20
$Fe_{58}B_6$	90.6	7.45	1.95	−0.17	1.75	1.93
		7.80	1.49	−0.13	1.34	1.48
		8.15	0.90	−0.08	0.81	0.89
$Fe_{55}B_9$	85.9	7.43	1.70	−0.14	1.44	1.67
$Fe_{51}B_{13}$	79.7	7.39	1.86	−0.14	1.45	1.82
		7.54	1.68	−0.13	1.31	1.64
		7.74	1.39	−0.11	1.09	1.39
$Fe_{48}B_{16}$	75.0	7.17	1.85	−0.14	1.35	1.8
$Fe_{42}B_{22}$	65.6	6.95	1.78	−0.14	1.12	1.70
		7.30	1.56	−0.12	0.99	1.51
		7.65	1.27	−0.09	0.80	1.22
$Fe_{32}B_{32}$	50.0	6.71	0.29	−0.02	0.14	0.28

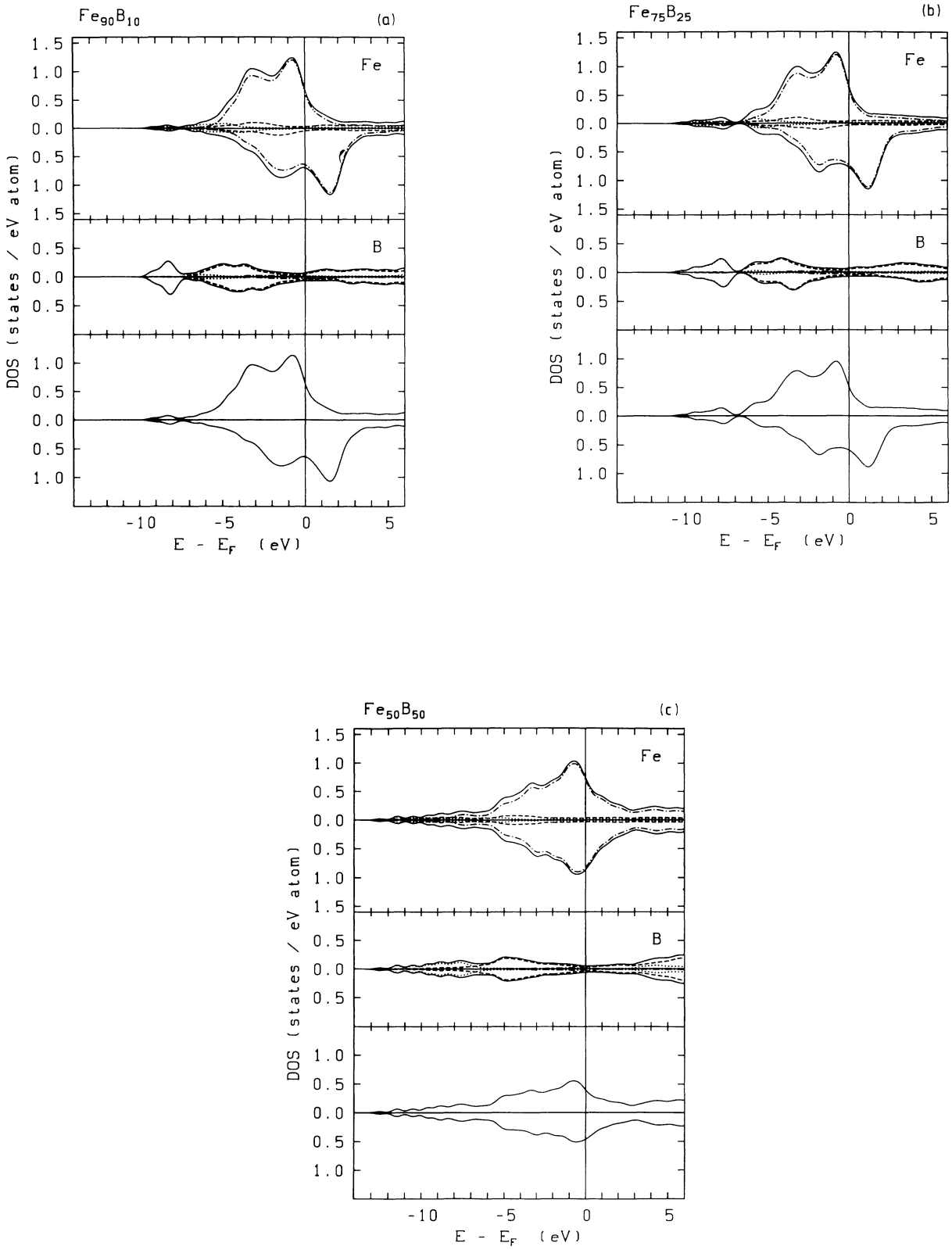

FIG. 4. Total, site, and angular momentum decomposed electronic density of states in amorphous $Fe_{90}B_{50}$ (a), $Fe_{75}B_{25}$ (b), and $Fe_{50}B_{50}$ (c). Solid lines, total (local) DOS; dotted line, partial *s*-electron DOS; dashed line, partial *p*-electron DOS; dot-dashed line, partial *d*-electron DOS.

C. Concentration dependence of the magnetic moment

Our calculations show that the variation of the magnetic moment of amorphous Fe_xB_{100-x} is dominated by two competing effects: (i) In the Fe-rich limit ($x \geq 80$) the magnetovolume effect is dominant. If the density data measured for amorphous samples with $82 \geq x \geq 88$ are extrapolated to lower B content (see Fig. 1), the average magnetic moment per Fe atom is predicted to be almost constant in this region (see Fig. 6). If the density is assumed to extrapolate to the density of bcc Fe (see Fig. 1), a decrease of the magnetic moment in the Fe-rich regime is predicted (see Fig. 6). Experimentally, all amorphous alloys with $x \geq 88$ are at least partially microcrystalline, with densities varying according to the preparation and the degree of cystallinity. The theoretical results, however, refer to purely amorphous systems. (ii) At larger B content the magnet moment decreases, essentially as a consequence of a dilution effect. Substitution of Fe by B leaves the Fe-Fe nearest-neighbor distance unchanged over a wide range of compositions, but reduces the number of Fe-Fe neighbors at a constant total coordi-

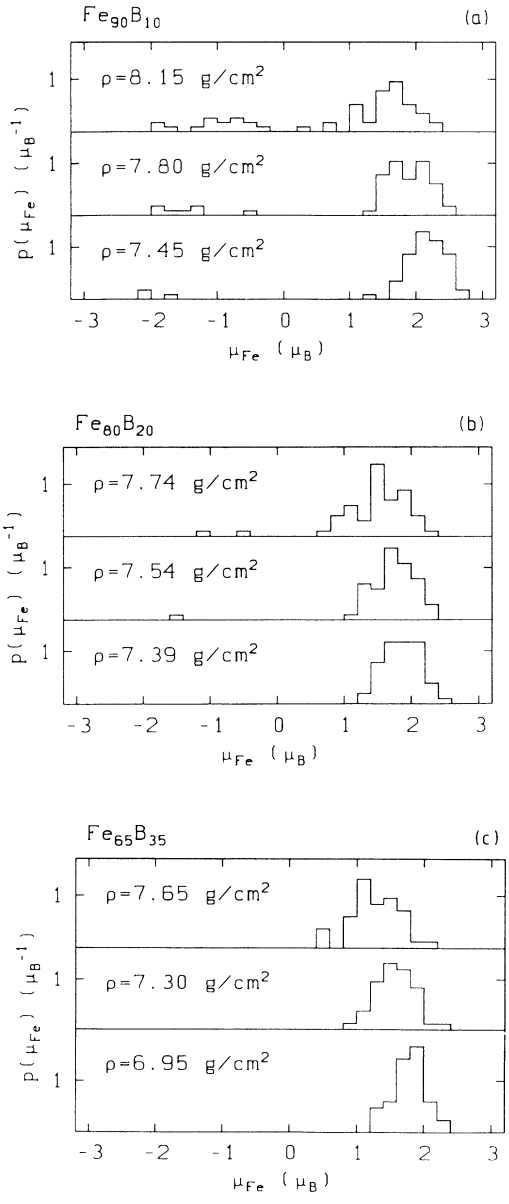

FIG. 5. Variation of the distribution of the local magnetic moments with density for amorphous $Fe_{90}B_{10}$ (a), $Fe_{80}B_{20}$ (b), and $Fe_{65}B_{35}$ (c). See text.

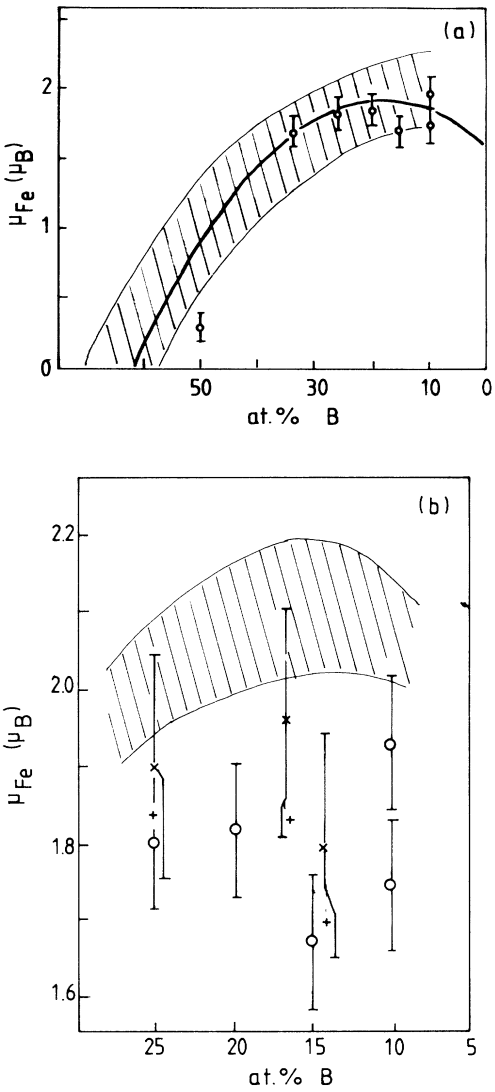

FIG. 6. Composition dependence of the average magnetic moment per Fe atom in a-Fe_xB_{100-x}: (a) Comparison with experimental data on thin amorphous films produced by sputtering or evaporation. The solid line represents an interpolation through the data of Bayreuther *et al.* (Ref. 13); the shaded area indicates the scatter of the experimental data compiled by Cowlam and Carr (Ref. 11). The open circles represent the results of the present calculations with the estimated error. The two values quoted for $Fe_{90}B_{10}$ correspond to the upper and lower limits of possible densities (cf. Fig. 1 and discussion). (b) Comparison with experimental data on melt-spun amorphous ribbons. The shaded areas summarize older experimental data compiled by Cowlam and Carr (Ref. 11). The more recent data of Ze *et al.* (Ref. 12) are represented by crosses: × (with error bars), neutron scattering; +, static magnetization measurements. The theoretical results are represented by the open circles.

nation number of the Fe sites.[35,36] As a consequence of the reduced number of Fe-Fe contacts, the *d*-band bonding becomes weaker. Instead the Fe-*d* states interact with the B-*p* states forming bonding and antibonding hybrids. The interaction with the B-*p* states pulls the Fe minority band down. This causes a rapid decrease of the magnetic moment per Fe atom to $\bar{\mu}(\mathrm{Fe})=0.50\mu_B$ in a $Fe_{50}B_{50}$ and to $\bar{\mu}(\mathrm{Fe})=1.22\mu_B$ in orthorhombic FeB.

Quite generally, the magnetization is weaker in the amorphous than in the crystalline alloys (see Table II). This is a consequence of the disorder-induced broadening of the *p-d* band complex which makes a large spin splitting energetically less favorable. At equal volume this would lead to a large reduction of the magnetic moment. However, the reduction of the density of the glassy phase relative to the crystal leads to an enhancement of the magnetization which compensates part of the disorder-induced reduction.

Comparison with experiment is complicated by the larger scatter of the published data.[11–15] Figure 6(a) compares our result with experimental data on thin amorphous films prepared by sputtering and coevaporation. The solid line gives an interpolation through the most reliable data;[13] the shaded area indicates the scatter of the other data given in the compilation of Cowlam and Carr.[11] The theoretical results are in excellent agreement with the experimental data; the slight underestimate of the magnetization in $Fe_{50}B_{50}$ is eventually due to the fact that the structural model is less realistic for these high B concentrations because of the neglect of the hybridization of B-*s* orbitals with the *p-d* band complex in the construction of the potential (see Sec. II). Experimental data on melt-spun amorphous ribbons are available only for B concentrations between 14 and 28 at. % B. Here we note a large discrepancy between the older data compiled by Cowlam and Carr and the more recent data obtained by Ze *et al.*[12] by neutron scattering and static magnetization measurements [Fig. 6(b)]. The new data are only slightly higher than the theoretical predictions.

Our calculations also explain why neither the band-gap model[7,8] nor the coordination-bond model[6] can be expected to work for *a*-Fe_xB_{100-x}. Both models make the fundamental assumption of strong ferromagnetism. This is simply incorrect because the Fermi level falls into a region of high DOS of the majority band. The weak magnetism is also confirmed by the strong magnetovolume effect. The calculations also do not confirm the existence of a hybridization gap that could pin the Fermi level.

D. Stoner model and local-moment criterion

In the Stoner model of itinerant ferromagnetism[2] the nonmagnetic state is unstable with respect to the formation of a ferromagnetic state if

$$I > \frac{1}{n(E_F)} . \tag{4.1}$$

Here I is the effective exchange integral and $n(E_F)$ is the DOS per atom and spin or equivalently the uniform Pauli susceptibility. The "Stoner parameter" I determines the exchange splitting Δ of spin-up and spin-down one-electron states as a function of the magnetic moment μ,

$$\Delta = I\mu . \tag{4.2}$$

This is a self-consistency equation: The exchange splitting produces spin-polarized electron states which add up to a net magnetic moment, and this has to satisfy the self-consistency relation (4.2). The Stoner model has originally been formulated for an elemental magnet. As in Fe_xB_{100-x} alloys, the B DOS at the Fermi level is negligible compared to the Fe DOS; the simple form of the model may be considered to be valid in the present case. The Stoner criterion has been generalized to local moments at impurity sites and to systems with disordered local moments.[62–64] In a disordered system, exchange splittings Δ_j on the sites $\mathbf{R}_j$ produce local moments[64]

$$\mu_i = \sum_j \chi_{ij}(E_F)\Delta_j + O(\Delta^3) , \tag{4.3}$$

where $\chi_{ij}(E_F)$ is the nonlocal susceptibility of the band electrons. Equation (4.3) holds for the ferromagnetic

TABLE II. Comparison of the magnetic moments calculated for amorphous and crystalline Fe_xB_{100-x} alloys.

		ρ (kg m^{-3})	μ_{Fe} (μ_B)	μ_{B} (μ_B)	$\bar{\mu}$ (μ_B)
Fe_3B	(orthorh)[a]	7.38	2.02,1.91	−0.263	1.39
	(orthorh)[b]	7.38	2.25,2.02	−0.15	1.53
$Fe_{75}B_{25}$	(am)	7.17	1.85	−0.14	1.35
Fe_2B	(tetr)[a]	7.36	1.95	−0.23	1.22
	(tetr)[c]	7.36	1.84	−0.11	1.19
$Fe_{65}B_{35}$	(am)	6.95	1.78	−0.14	1.12
		7.30	1.51	−0.12	0.97
FeB	(orthorh)[a]	6.71	1.26	−0.10	1.15
	(orthorh)[c]	6.71	1.25	−0.07	1.18
$Fe_{50}B_{50}$	(am)	6.71	0.29	−0.02	0.14

[a]Reference 45.
[b]Reference 44.
[c]Reference 43.

(FM), the antiferromagnetic (AFM), and the disordered local moment state. In a completely disordered state, splittings Δ_j and $-\Delta_j$ are equally probable on neighboring sites. Hence contributions from the neighbors average out, and the moment formation is determined by the purely local criterion

$$\mu_i = I(E_F)\Delta_i \ , \tag{4.4}$$

where $I(E_F)=\chi_{00}(E_F)$ is the local susceptibility. For the case of homogeneous FM or AMF, Eq. (3) becomes

$$\mu=\chi_{\rm FM}(E_F)\Delta=\Delta/n(E_F) \ , \tag{4.5}$$

$$\mu=\chi_{\rm AFM}(E_F)\Delta \ , \tag{4.6}$$

with the FM and AFM susceptibilities

$$\chi_{\rm FM}(E_F)=\sum_j \chi_{0j}(E_F) \ , \tag{4.7}$$

$$\chi_{\rm AFM}(E_F)=\sum_j r_j\chi_{0j}(E_F) \ , \tag{4.8}$$

$$r_j=\pm 1 \quad \text{for} \quad \Delta_j=\pm\Delta \ .$$

The FM and AFM criteria are then

$$I > 1/\chi_{\rm AFM} \tag{4.9}$$

for AFM and

$$I > 1/\chi_{\rm FM}=1/n(E_F) \tag{4.10}$$

for FM.

A generalization of the Stoner model to inhomogeneous amorphous magnets with fluctuating local moments and exchange splittings on the basis of (3) will hold if the proportionality between μ_i and Δ_i holds on a local level, i.e.,

$$\Delta_i = I\mu_i \ . \tag{4.11}$$

The validity of this relation seems plausible if the exchange splitting merely leads to a repopulation of states at the Fermi level, without changing the character of the occupied states (as happens for instance in an antiferromagnet). However, it is doubtful in a case of coexisting positive and negative local moments. The validity of this expression may be verified on the basis of our locally self-consistent LSD calculations. As the moment is carried predominantly by the Fe-3d states, we define the local exchange splitting Δ_i in terms of the difference in the position of the center of gravity $C_{{\rm R}_i nlm\downarrow(\uparrow)}$ of the spin-up and spin-down bands,

$$\Delta_i = C_{{\rm R}_i nlm\uparrow} - C_{{\rm R}_i nlm\downarrow}, \quad nl=3d \tag{4.12}$$

[this is also the convention adopted in a similar analysis for a-(Fe, Co, Ni)-Zr alloys[41]]. Within the LMTO ASA, the center of gravity is one of the potential parameters characterizing the one-electron potential within each muffin-tin sphere. Figure 7 shows the local exchange splitting Δ_i as a function of the local magnetic moment for all Fe sites in amorphous Fe_xB_{100-x} alloys with x varying between 95 and 50, and for different densities. We see that the proportionality expressed by Eq. (11) is obeyed exactly with $I=0.935$ eV/μ_B. This value is almost exactly the same as that found in crystalline and amorphous Fe-Zr and Co-Zr alloys (Fe, Co, and Zr sites) and in crystalline and amorphous Fe and Co ($I=0.95$ eV/μ_B).[41] This indicates that for d states the Stoner parameter is really a universal quantity. A similar conjecture was recently made by Himpsel[65] on the basis of photoemission and inverse photoemission data for a wide range of ferromagnetic, antiferromagnetic, and spin-glass systems. However, our result is more general, because it extends the correlation to the local moments and exchange splittings.

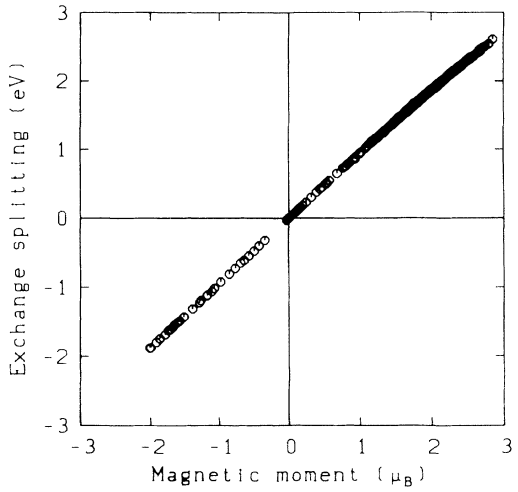

FIG. 7. Local exchange splitting against local moment μ_i for amorphous Fe_xB_{100-x} alloys with different compositions and densities (see text).

On the basis of this result it will be possible to extend Eqs. (4.6) and (4.7) to a criterion for local moment formation. With the local FM and AFM susceptibilities

$$\chi_{{\rm FM},i}(E_F)=\sum_j \chi_{ij}(E_F) \ , \tag{4.13}$$

$$\chi_{{\rm AFM},i}(E_F)=\sum_j r_j\chi_{ij}(E_F) \ , \tag{4.14}$$

a site i will acquire a positive moment if

$$\chi_{{\rm AM},i} > \chi_{{\rm AFM},i} > 1/I \tag{4.15}$$

and a negative moment if

$$\chi_{{\rm AFM},i} > \chi_{{\rm FM},i} > 1/I \ . \tag{4.16}$$

The calculation of the local susceptibilities is now under way.

E. Photoemission spectroscopy

Photoemission spectroscopy should in principle provide a critical test of the theoretical predictions on the electronic structure. For amorphous solids, the situation is complicated by the fact that the electronic DOS shows no sharp features like the Van Hove singularities of the spectrum of crystalline materials that could be related to

the corresponding features in the photoemission intensity. Hence the analysis must be based on a quantitative comparison of the calculated and measured intensities. These are given by

$$I(E)=\sum_{\alpha,l,\sigma}\sigma_{\alpha l\sigma}(\hbar\omega,E)n_{\alpha l\sigma}(E),\quad \alpha=\text{Fe, B}\ , \qquad (4.17)$$

where the $n_{\alpha l\sigma}(E)$ are the spin-polarized partial local densities of state and the $\sigma_{\alpha l\sigma}(\hbar\omega,E)$ are the partial photoionization cross sections calculated in a single-scatterer final-state approximation.[50,51,66] Equation (14) allows for an accurate calculation of the theoretical spectra. The problem is now rather in the processing (background subtraction, etc.) of the experimental spectra. This appears to be particularly difficult for a-Fe_xB_{100-x}, where the available experimental data are widely different.[24–27] The calculated photoemission intensities for ultraviolet photoemission spectroscopy [(UPS) $\hbar\omega=21.2$ eV] and x-ray photoemission spectroscopy [(XPS) $\hbar\omega=1486.6$ eV] are shown in Fig. 8. The calculated spectra have been folded with a Gaussian resolution function ($\sigma=0.3$ eV for XPS, $\sigma=0.1$ eV for UPS). Both series of spectra show a peak within 1 eV from the Fermi energy, a shoulder at 3–3.5 eV binding energy, and a further maximum at ~ -8 eV. The first peak and the shoulder correspond to the two-peak structure of the majority band. The single peak in the DOS of the occupied minority states falls in between these two peaks (see Fig. 2); this reduces the structure visible in the photoemission intensities. The peak at -8 eV arises from B-s states. The difference between UPS and XPS spectra arises from the reduced photoionization cross section for B and the faster decay of the Fe cross section with increasing binding energy in the UPS regime. Figure 9 shows a comparison of theoretical and experimental spectra for $Fe_{75}B_{25}$. There is an overall agreement, but also substantial differences in the details. Theory predicts a DOS maximum within 1 eV below the Fermi level. This seems to agree with the XPS data of Cartier *et al.*[27] and (within very low experimental resolution) Matsuura *et al.*[24] and with the UPS data of Amamou and Krill,[26] whereas the XPS data of Amamou and Krill and the UPS ($\hbar\omega=21.2$ eV) data of Paul and Neddermeyer[25] seem to show a second peak at or slightly above E_F. Paul and Neddermeyer also investigated the variation of the UPS spectra with the energy of the exciting photon ($\hbar\omega=16.8$–40.8 eV) and found variations in the intensities that could be explained only assuming large variations of the cross sections over small intervals of the binding energy. This seems unrealistic. There is also no systematic in the features observed at higher binding energies. It seems to be fair to say that more accurate experimental data are needed.

x-ray emission spectra[28,29] confirm that there are only small differences in the d bands of crystalline and amorphous Fe-B, and also only small variations relative to pure Fe. However, the resolution of the spectra is certainly insufficient to allow for a critical test of the theoretical predictions.

The calculated linear coefficient γ for the electronic specific heat lies below the experimental data,[23] but is substantially higher than the paramagnetic results of

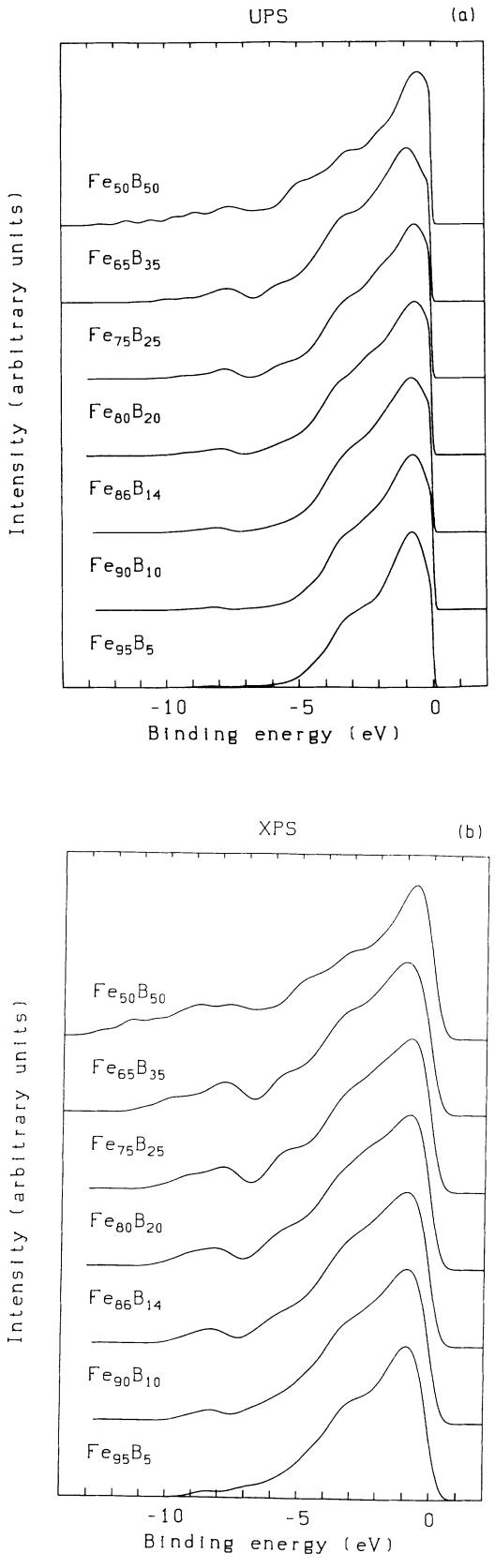

FIG. 8. Theoretical ultraviolet (a) ($\hbar\omega=21.2$ eV) and x-ray (b) ($\hbar\omega=1486.6$ eV) photoemission intensities for ferromagnetic Fe_xB_{100-x} alloys.

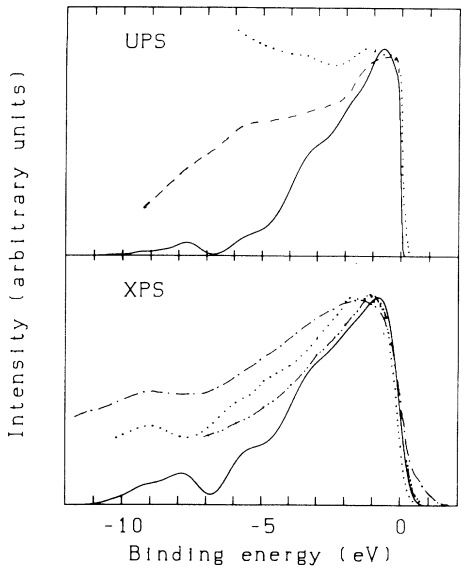

FIG. 9. Comparison of calculated and experimental UPS (a) and XPS (b) spectra for $Fe_{75}B_{25}$. Solid lines, theory; dashed line, Paul and Neddermeyer (Ref. 25); dotted line, Amamou and Krill (Ref. 26); dot-dashed line, Matsuura *et al.* (Ref. 24); double dot–dashed line, Cartier *et al.* (Ref. 27).

Fujiwara[17] and Nowak *et al.*[18] (see Fig. 10). The remaining difference can be explained in terms of spin fluctuations, with realistic results for the enhancement factor λ_{spin}. It is characteristic that λ_{spin} increases in the Fe-rich limit.

V. CONCLUSIONS

We have presented self-consistent spin-polarized electronic-structure calculations for amorphous Fe_xB_{100-x} alloys, based on realistic models of the atomic structure. Our calculations show that the electronic density of states of the amorphous alloys is very similar to that of the crystalline Fe borides: The electronic states close to the Fermi level are dominated by Fe-*d* states that are strongly hybridized with the B-*p* states. A distinct hybridization gap separates the bottom of the Fe-*d*–B-*p* band complex from a nonbonding B-*s* band. This shows that the basic assumptions made in the calculation of the interatomic forces using the tight-binding-bond model[35] are correct. The similarity of the electronic structures of the crystalline and amorphous phases corroborates the conclusions drawn on the basis of the computer simulations of the atomic structure: The local order (both chemical and topological) in the glassy phase is similar to the trigonal prismatic crystalline structures. We have also presented detailed calculations of the photoemission intensities. However, the comparison with the available experimental data reveals large discrepancies among the various sets of experiments. More reliable experiments are needed to permit a critical evaluation of the theoretical predictions. The calculated DOS at the Fermi level agrees well with low-temperature specific-heat data if the electron-photon and spin-fluctuation enhancement factors are taken into account.

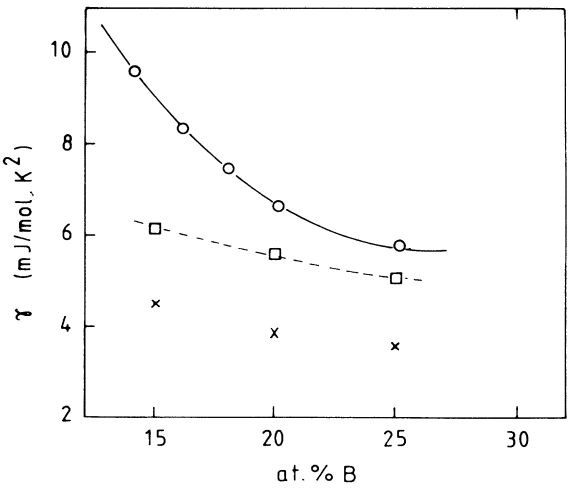

FIG. 10. Linear coefficient of the electronic specific heat for *a*-Fe_xB_{100-x}. ○, experiment (Ref. 23); □, present calculation (spin polarized); ×, Fujiwara (Ref. 17) and Nowak *et al.* (Ref. 18), non-spin-polarized calculation.

The predicted composition dependence of the magnetic moments agrees very well with data on thin amorphous films and reasonably well with the most recent data on melt-spun amorphous ribbons. Older data on melt-spun samples point to somewhat higher magnetic moments than the theoretical predictions. For the Fe-rich alloys we find a large magnetovolume effect. The analysis of the physical effects involved in the variation of the magnetic moment with composition shows that the situation is far more complex than predicted either by the coordination-bond model[6] or the band-gap theory:[7,8] In the Fe-rich limit, the magnetic moment is reduced relative to that of bcc Fe, because fluctuations in the local atomic environment lead to a competition between ferro- and antiferromagnetic exchange interactions. The interactions leading to the formation of negative local moments on Fe sites are extremely sensitive to local charge self-consistency: Averaging over the charge density calculated at different sites eliminates the local moments. Therefore the negative Fe moments have not been seen in previous calculations based on empirical TB Hamiltonians,[19] in non-self-consistent calculations,[20] or in calculations achieving self-consistency only on an average atom.[60] The negative Fe moments disappear for B contents larger than 15%, leading to a maximum moment per Fe atom close to this composition. At larger B content, the magnetic moment is reduced, because polarizable *d*-*d* bonds are replaced by magnetically inert *p*-*d* bonds.

Our calculations for the Fe-B glasses confirm results obtained on inter-transition-metal glasses[41] and on amorphous iron[16] that there is a universal proportionality of the local magnetic moments and the local exchange splitting—the Stoner parameter is a constant for itinerant 3*d* magnets, even on a local level.

Our results show that the LMTO supercell technique is a reliable tool for predicting the electronic and magnetic properties of topologically disordered materials, without any adjustable parameters. Remaining problems are the precise nature of the mechanism giving rise to negative

moments and the effect of these frustrated interactions on the spin structure: Exactly antiparallel moments on a disordered structure are necessarily an oversimplification. In both respects the last result of a universal *local* Stoner parameter will be important: It allows one to transform to a local TB-LMTO Hamiltonian and to formulate a local moment criterion for glassy alloys, as well as to relax the condition of collinear spin structures. These results will be reported soon.

ACKNOWLEDGMENT

This research has been supported by the Bundesministerium für Wissenschaft und Forschung under Contract No. 49.787/2-24/92.

[1]For recent reviews, see, e.g., K. Moorjani and J. M. D Coey, *Magnetic Glasses* (Elsevier, Amsterdam, 1984); *The Magnetism of Amorphous Metals and Alloys,* edited by J. A. Fernandez-Boca and W. Y. Ching (World Scientific, Singapore, 1993).

[2]E. C. Stoner, Prog. R. Soc. London A **154**, 656 (1936); E. P. Wohlfarth, Rev. Mod. Phys. **25**, 211 (1953).

[3]V. Korenman and R. E. Prange, Phys. Rev. B **19**, 4691 (1979); **19**, 4698 (1979).

[4]W. Heisenberg, Z. Phys. **49**, 619 (1928).

[5]T. Kaneyoshi, *Introduction to Amorphous Magnets* (World Scientific, Singapore, 1992).

[6]B. W. Corb, R. C. O'Handley, and N. J. Grant, Phys. Rev. B **27**, 636 (1983).

[7]A. P. Malozemoff, A. R. Williams, K. Terakura, V. L. Moruzzi, and K. Fukamishi, J. Magn. Magn. Mater. **35**, 192 (1983).

[8]A. P. Malozemoff, A. R. Williams, and V. L. Moruzzi, Phys. Rev. B **29**, 1620 (1984).

[9]F. Stein and G. Dietz, J. Magn. Magn. Mater. **117**, 45 (1992).

[10]T. Egami, Rep. Prog. Phys. **32**, 311 (1988).

[11]N. Cowlam and G. E. Carr, J. Phys. F **15**, 1109 (1975); **15**, 1117 (1975).

[12]Ze Xianyu, Y. Ishikawa, F. Fukunaga, and N. Watanabe, J. Phys. F **15**, 1799 (1985).

[13]H. Hoffmann, M. Takahashi, and J. Zweck, J. Magn. Magn. Mater. **35**, 211 (1983); B. Bayreuther, G. Enders, H. Hoffmann, V. Korndörfer, W. Oesterreicher, K. Röll, and M. Takahashi, J. Magn. Magn. Mater. **31-34**, 1535 (1983).

[14]T. Stobiecki and F. Stobiecki, J. Magn. Magn. Mater. **35**, 217 (1983).

[15]K. H. J. Buschow and P. G. van Engen, J. Appl. Phys. **52**, 3557 (1982).

[16]I. Turek and J. Hafner, Phys. Rev. B **46**, 247 (1992).

[17]T. Fujiwara, J. Non-Cryst. Solids **61+62**, 1039 (1984).

[18]H. K. Nowak, O. K. Andersen, T. Fujiwara, O. Jepsen, and P. Vargas, Phys. Rev. B **44**, 3577 (1991).

[19]S. Krompiewski, U. Krey, U. Krauss, and H. Ostermeier, J. Magn. Magn. Mater. **73**, 5 (1988); **69**, 117 (1987).

[20]W. Y. Ching and Y. N. Xu, J. Appl. Phys. **70**, 6305 (1991).

[21]I. Turek, J. Phys. Condens. Matter **2**, 10559 (1990).

[22]O. K. Andersen and O. Jepsen, Phys. Rev. Lett. **53**, 2571 (1984); O. K. Andersen, O. Jepsen, and M. Šob, in *Electronic Band Structure and its Applications,* edited by M. Yussouff, Lecture Notes in Physics Vol. 283 (Springer, Berlin, 1987).

[23]M. Matsuura, V. Mizutani, and Y. Yazawa, J. Phys. F **11**, 1393 (1981).

[24]M. Matsuura, T. Nomoto, F. Itoh, and K. Suzuki, Solid State Commun. **33**, 895 (1980).

[25]T. Paul and H. Neddermeyer, J. Phys. F **15**, 79 (1985).

[26]A. Amamou and G. Krill, Solid State Commun. **33**, 1087 (1980).

[27]E. Cartier, Y. Baer, M. Liard, and H. J. Güntherodt, J. Phys. F **10**, L21 (1980).

[28]K. Tanaka, M. Yoshino, and K. Suzuki, J. Phys. Soc. Jpn. **51**, 3882 (1982).

[29]S. Falch, G. Rainer-Harbach, F. Schmückle, and S. Steeb, Z. Naturforsch. **36a**, 937 (1981).

[30]C. A. Coulson, Proc. R. Soc. London A **169**, 413 (1939).

[31]D. G. Pettifor, Phys. Rev. Lett. **63**, 2480 (1989).

[32]D. G. Pettifor and M. Aoki, Philos. Trans. R. Soc. London A **334**, 439 (1991).

[33]Ch. Hausleitner and J. Hafner, Phys. Rev. B **42**, 5863 (1990).

[34]Ch. Hausleitner and J. Hafner, Phys. Rev. B **45**, 115 (1992); **45**, 128 (1992).

[35]Ch. Hausleitner and J. Hafner, Phys. Rev. B **47**, 5689 (1993).

[36]Ch. Hausleitner, J. Hafner, and Ch. Becker, Phys. Rev. B **48**, 13 119 (1993).

[37]S. S. Jaswal and J. Hafner, Phys. Rev. B **38**, 3711 (1988); **38**, 7320 (1988).

[38]J. Hafner and W. Jank, Phys. Rev. B **45**, 2739 (1991); and references cited therein.

[39]S. K. Bose, S. S. Jaswal, O. K. Andersen, and J. Hafner, Phys. Rev. B **37**, 9955 (1988).

[40]H. Yang, J. C. Swihart, D. M. Nicholson, and R. H. Brown, Phys. Rev. B **47**, d107 (1993).

[41]I. Turek, Ch. Becker, and J. Hafner, J. Phys. Condens. Matter **4**, 7257 (1992).

[42]J. Hafner, Ch. Hausleitner, W. Jank, and I. Turek, J. Non-Cryst. Solids **150**, 307 (1992).

[43]P. Mohn and D. G. Pettifor, J. Phys. C **21**, 2829 (1988); **21**, 2829 (1988).

[44]M. Tegze, R. A. de Groot, F. van der Woude, and F. M. Mueller, in *Rapidly Quenched Metals V,* edited by S. Steeb and H. Warlimont (North-Holland, Amsterdam, 1985), p. 1031.

[45]W. Y. Ching, Y. N. Xu, B. N. Harmon, J. Ye, and T. C. Leung, Phys. Rev. B **42**, 4460 (1990).

[46]M. A. St. Peters and L. M. Roth, J. Non-Cryst. Solids **75**, 455 (1985).

[47]R. Lorenz and J. Hafner (unpublished).

[48]H. L. Skriver, *The LMTO Method* (Springer, Berlin, 1984).

[49]U. von Barth and L. Hedin, J. Phys. C **5**, 1629 (1972).

[50]T. Jarlborg and P. O. Nilsson, J. Phys. C **12**, 265 (1979).

[51]J. Redinger, P. Marksteiner, and P. Weinberger, Z. Phys. B **63**, 321 (1986).

[52]R. Hasegawa and R. Ray, J. Appl. Phys. **49**, 4174 (1978).

[53]P. Gaskell, in *Metallic Glasses II,* edited by H. Beck and H. J. Güntherodt (Springer, Berlin, 1983), p. 1.

[54]R. W. G. Wyckoff, *Crystal Structures,* 2nd ed. (Wiley, New York, 1963).

[55]P. Mohn and K. Schwarz, Physica **130B**, 26 (1985).

[56]Y. Kakehashi, Phys. Rev. B **43**, 10820 (1991).

[57]E. S. Wang, B. M. Klein, and H. Krakauer, Phys. Rev. Lett. **54**, 1852 (1985).

[58]V. L. Moruzzi, P. M. Marcus, and J. Kübler, Phys. Rev. B **39**, 6957 (1989).

[59]J. Kübler, Solid State Commun. **72**, 631 (1989).

[60]A. M. Bratkovsky and A. V. Smirnov, J. Phys. Condens.

Matter **5**, 3203 (1993).
[61]Ch. Becker and J. Hafner (unpublished); R. Lorenz and J. Hafner (unpublished).
[62]D. G. Pettifor, J. Magn. Magn. Mater. **15-18**, 847 (1980).
[63]V. Heine, J. H. Samson, and C. M. M. Nex, J. Phys. F **11**, 2645 (1981).
[64]V. Heine and J. H. Samson, J. Phys. F **13**, 2155 (1983).
[65]F. Himpsel, Phys. Rev. Lett. **67**, 2363 (1991).
[66]W. Jank and J. Hafner, J. Phys. Condens. Matter **2**, 5065 (1990).